CrossMark

RESEARCH PAPER

Brittle fracture assessment of embedded flaw in heat-affected zone based on Weibull stress criterion

Y. Seko[1] · Y. Imai[1] · M. Mitsuya[2] · N. Oguchi[2] · F. Minami[3]

Abstract This paper presents a method for estimating the condition for the brittle fracture limit of a welded joint with an embedded flaw in the heat-affected zone (HAZ) based on the Weibull stress criterion. A welded joint with an embedded flaw generated by cold cracking was subjected to a wide plate (WP) tension test, and a welded joint with a fatigue crack was subjected to three-point bending (3PB) tests; both tests were conducted at −30 °C. Brittle fractures occurred in all specimens, and the microstructure of the fracture initiation point for the WP specimen in the coarse-grained HAZ (CGHAZ) was upper bainite with M-A constituents. The critical Weibull stress distribution of the CGHAZ was calculated by finite element analyses for the 3PB specimens. The predicted fracture load and global displacement of the WP specimen at the brittle fracture obtained by the critical Weibull stress distribution were in agreement with experimental results from the WP tensile test. This confirmed that the brittle fracture limit of a welded joint with an embedded flaw could be predicted from the Weibull stress criterion.

Recommended for publication by Commission X - Structural Performances of Welded Joints - Fracture Avoidance

✉ Y. Seko
  y.seko@tokyo-gas.co.jp

[1] Fundamental Technology Research Institute, Tokyo Gas Co., Ltd, Yokohama, Japan

[2] Transmission Pipeline Group, Tokyo Gas Co., Ltd, Tokyo, Japan

[3] Joining and Welding Research Institute, Osaka University, Ibaraki Osaka, Japan

1 Introduction

Welding is widely used in the construction of infrastructure, such as factories, vessels, and bridges. To ensure the safety of the infrastructure after welding, welding flaws that are detected during non-destructive inspections should be eliminated. However, it is not reasonable to remove all the welding flaws, including microscopic flaws that do not affect the brittle fracture of a structural component. Standards for fracture toughness assessment, such as BS7910 and WES2805, have been used to evaluate the brittle fracture of the detected welding flaws [1, 2]. However, these standards sometimes provide an excessively conservative safety assessment owing to the difference in the plastic constraint of the materials.

To solve this problem, the Weibull stress has recently been used as a fracture-driving force against brittle fracture assessment. The Weibull stress has been shown to be independent of size and geometry [3, 4]. A constraint-loss correction procedure that uses the Weibull stress criterion was specified as ISO 27306 in 2009 [5]. This standard provides the equivalent critical crack tip opening displacement (CTOD) ratio, β, for the brittle fracture assessment of a structural component with a flaw, based on the Weibull stress criterion. However, ISO 27306 is applicable to the assessment of flaws in the base metal.

The Weibull stress criterion has been applied to assessments of a welded joint [6–8]. For example, Minami applied the Weibull stress criterion to brittle fracture assessment of an X80 steel weld with a surface notch. Yamashita presented the effect of welding residual stress on brittle fracture of a welded joint with a through notch based on the Weibull stress criterion. However, these studies are limited to surface or through notches, and to the best of our knowledge, there have been no studies on the application of the Weibull stress criterion to an embedded flaw.

Table 1 Chemical composition of the 780-MPa class high-strength steel plate (mass %)

C	Si	Mn	P	S	Cu	Ni	Cr
0.13	0.24	0.91	0.008	0.007	0.31	0.09	1.03
Mo	V	B	O	N	C_{eq}	P_{cm}	
0.48	0.005	0.002	0.002	0.014	0.62	0.28	

$C_{eq} = C + Mn/6 + (Cr + Mo + V)/5 + (Ni + Cu)/15$

$P_{cm} = C + Si/30 + (Mn + Cu + Cr)/20 + Ni/60 + Mo/15 + V/10 + 5B$

In this study, the Weibull stress criterion is applied to brittle fracture assessment of a welded joint with an embedded crack generated by cold cracking. The applicability is clarified by experiments and finite element analyses, and the effect of welding residual stress and crack configuration on Weibull stress is investigated.

## 2 Wide plate tensile test of welded joint with an embedded crack generated by cold cracking

This chapter briefly explains the results of a wide plate tensile test of a welded joint with an embedded crack conducted by Imai [9]. The test method and detailed results are described in the cited paper.

2.1 Manufacturing welded joint with cold cracking

In this study, a 780-MPa class high-strength steel plate with a thickness of 25 mm was used. Its chemical composition is listed in Table 1. Welded joints were made by shielded metal arc welding under the conditions listed in Table 2. This welding condition leads to cold cracking inside the plate, as shown in Fig. 1. The mechanical properties of the base and weld metal at −30 °C are listed in Table 3. The yield stress of the weld metal was approximately 0.83 times than that of the

Table 2 Welding condition for the WP specimen

Welding method		SMAW
Groove geometry		K-groove
Welding consumable material		JIS Z 3211 E7816-N5CM3U
Number of passes		13
1st layer	Welding current	200 A
	Welding voltage	24 V
	Pre-heat temperature	without
Subsequent layers	Welding current	180~200 A
	Welding voltage	24~25 V
	Pre-heat temperature	180 °C
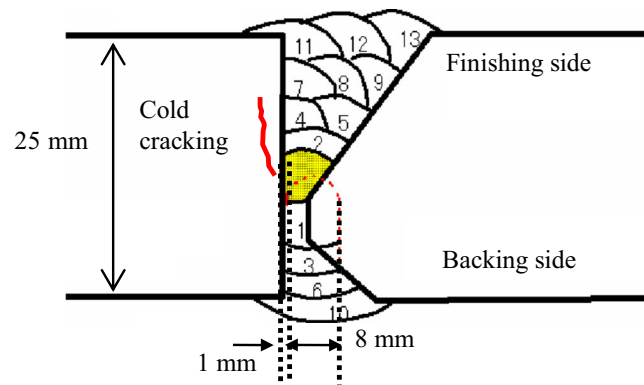
Fig. 1 Schematic of the cross section of the weld

base metal, whereas the tensile strength of the weld metal was slightly smaller than that of the base metal.

2.2 Test method

Figure 2 shows the configuration of wide plate tensile specimen having a welded joint with embedded cold cracking. The test section of this specimen was 350-mm long and 195-mm wide. The test specimen was tensioned along the direction normal to the weld line at −30 °C. The tension rate was approximately 0.6 mm/min, and the tension load and global displacement were measured during the experiment.

2.3 Test result

Figure 3 shows the relationship between the tension load and the global displacement (finishing side). A brittle fracture occurred at 3584 kN after plastic deformation. A pop in was not observed during the experiment. Figure 4a shows the fracture surface of the test specimen. The crack depth from the finishing side varied with respect to the width direction. The maximum crack height was 10.8 mm, and the crack length was approximately 80 mm.

The location of the brittle fracture initiation point is indicated in Fig. 4a, b, c. The initiation point was located in the coarse-grained heat-affected zone (CGHAZ), which is

Table 3 Mechanical properties of the base and weld metal at −30 °C

	Yield stress (MPa)	Tensile strength (MPa)	Elongation (%)	Yield ratio (%)
Base metal	795	870	21	91
Weld metal	661	823	41	80

Fig. 2 Schematic of the test specimen
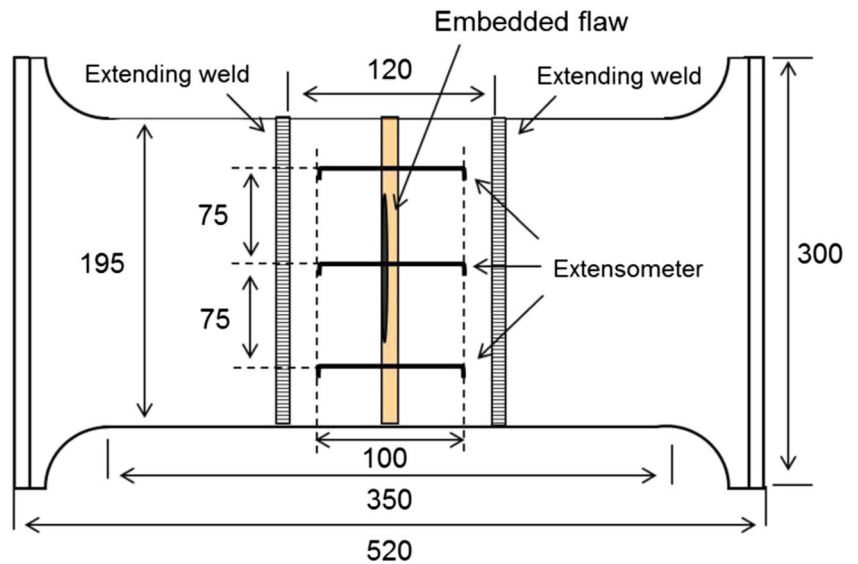
0.12 mm from the bond line. Figure 5 shows the microstructure at the fracture initiation point according to API RP 2Z [11]. The microstructure at the fracture initiation point was upper bainite with M-A constituents, and the grain-size was approximately 100 μm.

3 Critical Weibull stress distribution

The critical Weibull stress distribution of the targeted welded joint is necessary for brittle fracture assessment based on the Weibull stress criterion. In this chapter, three-point bend tests were performed on the welded joint, which has the same mechanical properties as that of the welded joint for the WP specimen. Then, the critical Weibull stress distribution was calculated by finite element analyses.
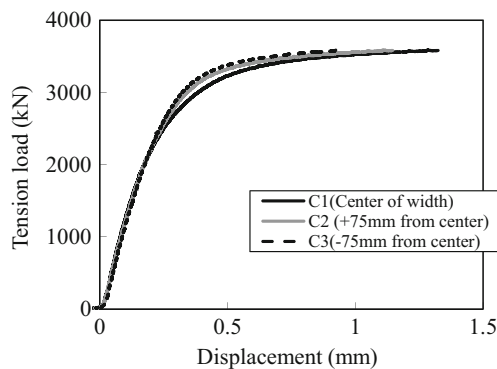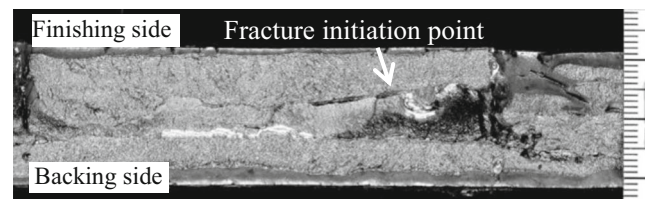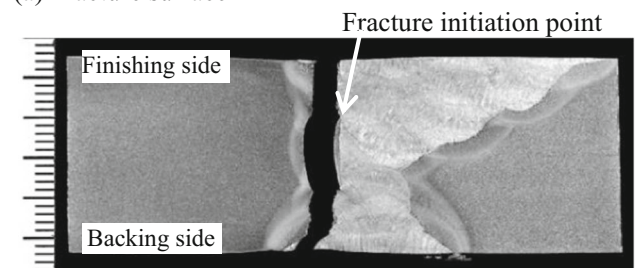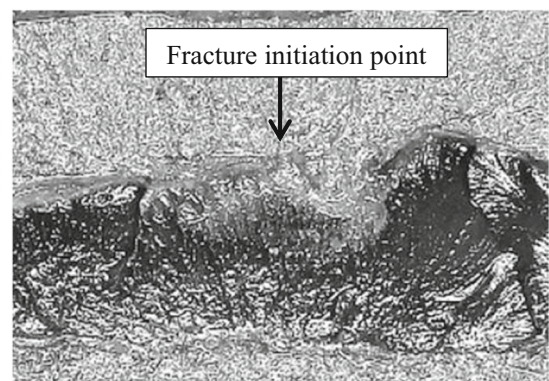

(a) Fracture surface

(b) Cross section of the weld

(c) Enlarged view around the fracture initiation point

Fig. 4 Test specimen after brittle fracture. **a** Fracture surface. **b** Cross section of the weld. **c** Enlarged view around the fracture initiation point
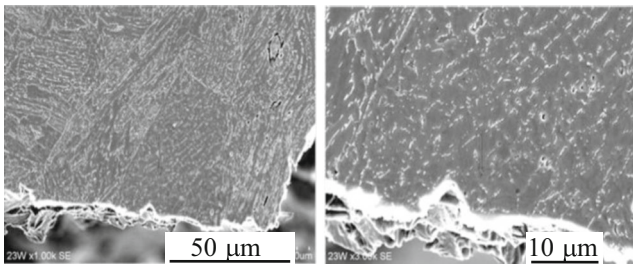

Fig. 3 Load–displacement curves

Fig. 5 Microstructure at the fracture initiation point

Table 4 Welding conditions

Welding method	SMAW
Groove geometry	K-groove
Welding consumable material	JIS Z 3211 E7816-N5CM3U
Number of passes	13
Welding current	180∼200 A
Welding voltage	24∼25 V
Pre-heat temperature	150∼180 °C

3.1 Three-point bending test

3.1.1 Manufacturing welded joint without flaw

Shielded metal arc welding was used to create the joint without a flaw, under conditions listed in Table 4. The heat input, groove geometry, and number of passes of this welded joint are almost the same as that of the welded joint
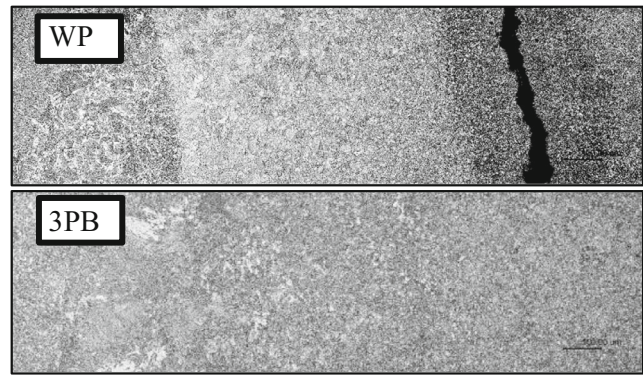

Fig. 7 Microstructures of CGHAZ

with cold cracking for the WP specimen. On the other hands, there are difference points for the restraint condition and the pre-heat temperature of 1st layer. For the WP specimen, the restraint weld was introduced at outside of weld with cold cracking before introducing weld with cold cracking, and preheating of 1st layer was not conducted to generate cold cracking [9]. For the 3PB specimen, the restraint weld was not introduced, and preheating of 1st layer was conducted at 180 °C.

Figure 6 shows a comparison of the Vickers hardness distribution between the welded joint with cold cracking for WP specimen and that without cold cracking for the three-point bending (3PB) specimen. In addition, Fig. 7 shows the microstructure of the CGHAZ near the bond line. The mechanical properties of the 3PB specimen were almost the same as that of the WP specimen because the Vickers hardness distribution and microstructure of CGHAZ of both specimens were almost the same.

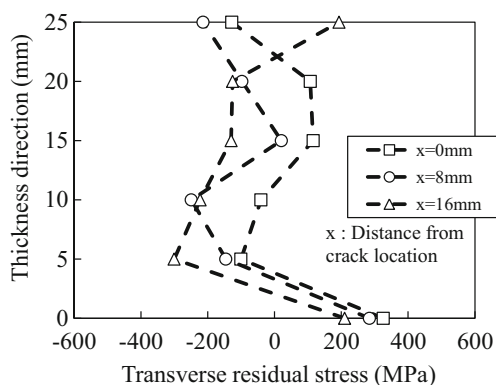**Fig. 6** Vickers hardness distribution
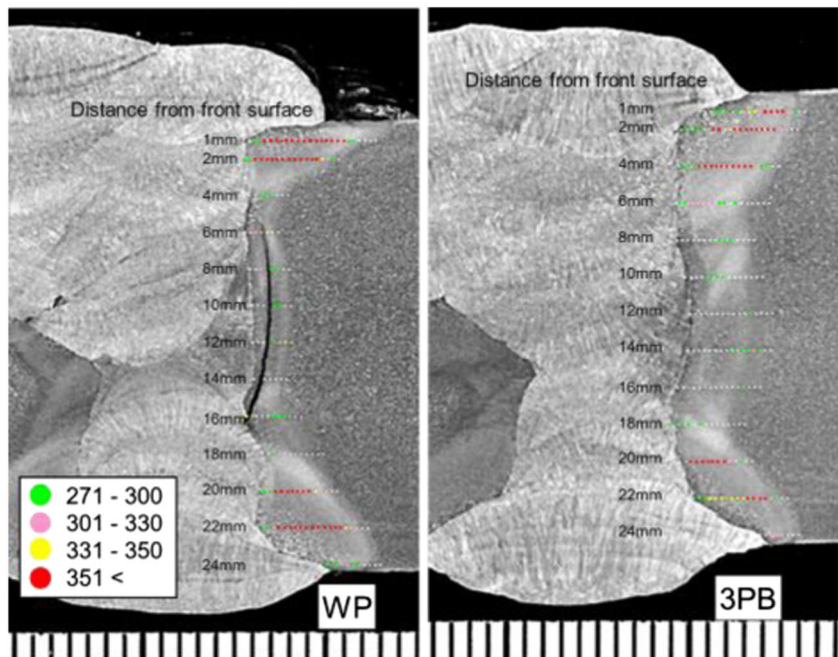
Fig. 8 Distribution of transverse residual stress measured by the released strain method

Figure 8 shows the distribution of the transverse welding residual stress in the thickness direction, which was measured by the released strain method [10]. The measured lines were located at the center of the weld line, 8 and 16 mm from the weld line. The maximum tensile residual stress at the surface was approximately 0.4 times the base metal yield stress, and compressive residual stress was present near the center of the thickness direction.

3.1.2 Test method

Twenty 3PB tests were conducted at −30 °C. Figure 9 shows the geometry of the 3PB specimen extracted from the welded joints. The 3PB specimen had a through-thickness notch. The ratio of the notch depth including the fatigue crack to the specimen width, a/W, was 0.5. First, the machined notch was introduced at the HAZ near the fusion lines, and then, a fatigue crack was introduced at the machined notch tip by bending. The fatigue crack length of the 3PB specimen was approximately 2.5 mm. The notch tip included the CGHAZ.

The load and the crack mouth opening displacement (CMOD) were measured during the experiment. The loading span was 200 mm. The CTOD of the 3PB specimen, δ_{3PB}, was calculated according to BS7448 by the following equation [11]:

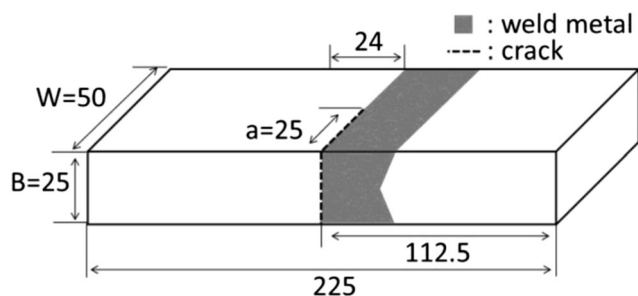$$\delta_{3PB} = \frac{K^2(1 - \nu^2)}{2\sigma_y E} + \frac{0.4(W - a)v_p}{0.4W + 0.6a + z} \quad (1)$$
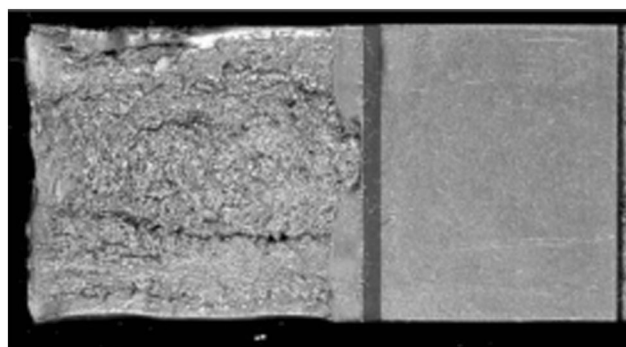

Fig. 9 Geometry of the 3PB specimen

Fig. 10 Fracture surface of the 3PB specimen (Y17)

where K, ν, σ_y, and E are the stress intensity factor, Poisson ratio, yield stress, and Young's modulus, respectively. W, a, v_p, and z are the specimen width, notch length including fatigue crack, plastic component of the crack mouth opening displacement, and height of the knife edge above the crack mouth, respectively.

After testing, all specimens were subjected to a sectioning procedure according to API RP 2Z [12] in order to identify the notch tip location and the microstructure at the fracture initiation point.

3.1.3 Test result

Brittle fracture occurred in all specimens. Figure 10 shows the fracture surfaces of the 3PB specimen, Y17, which had a critical CTOD of 0.030 mm. Owing to small fatigue crack growth near the center of thickness direction, the crack tip exhibited a snaked shape in the thickness direction. Fifteen specimens were invalid as per BS 7448 owing to the crack front shape. The fatigue crack growth was prevented by compressive residual stress generated near the center of thickness direction, as shown in Fig. 8. In addition, the fracture initiation points were located near the snaked crack tip region owing to stress concentration.

Figure 11 shows the relationship between the critical CTOD and the cumulative fracture probability. The figure legend shows the microstructure of the fracture initiation point. Thirteen specimens were fractured at the CGHAZ.
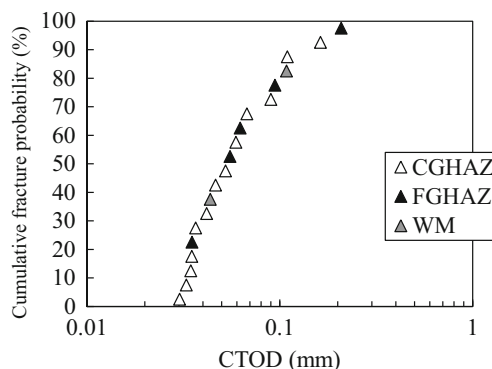

Fig. 11 Critical CTOD of the 3PB specimens at brittle fracture initiation

The critical CTOD of the specimens with fractures at the CGHAZ tended to be lower than that of the other specimens.

3.2 Finite element analysis

3.2.1 Analysis procedure

In this study, the fracture process zone was limited to the CGHAZ region because the WP specimen fractured in that region. Therefore, 3PB finite element analyses were conducted for thirteen specimens fracturing in CGHAZ.

ABAQUS ver. 6.11.5 was used for finite element analysis (FE analysis; FEA). Figure 12 shows the FE meshes used for the 3PB specimens. The minimum element size at the crack tip was $0.025 \times 0.025 \times 0.2$ mm. Iso-parametric elements with eight nodes, C3D8, were employed. The analytical model was classified into four parts for material properties based on the hardening distribution shown in Fig. 6: the base metal, weld metal, HAZ, and softened HAZ. Both microstructure distribution and crack front shapes of each model were individually configured based on the original specimen.

Figure 13 shows the relationship between true stress and true plastic strain employed in the FEA. This relationship for the base and weld metal parts was calculated from the results of round bar tensile tests. The stress–strain relationship for the HAZ region was estimated by the Vickers hardness ratio between HAZ and base metal. CTOD was calculated using Eq. (1).

Welding residual stress was not introduced FE model for 3PB specimen because residual stress does not affect the Weibull stress as crack driving force for 3PB specimen [13].

3.2.2 Weibull stress criterion

The Weibull stress criterion was used for the assessment of the fracture-driving force. The Weibull stress, σ_w, is defined by the following equation:

$$\sigma_w = \left[\frac{1}{V_0} \int_{V_f} (\sigma_{\text{eff}})^m dV_f \right]^{\frac{1}{m}} \quad (2)$$

where V_0 is a reference volume defined for the Weibull stress, σ_{eff} is an effective stress normally represented by the maximum principal stress, m is a shape parameter, and V_f is the
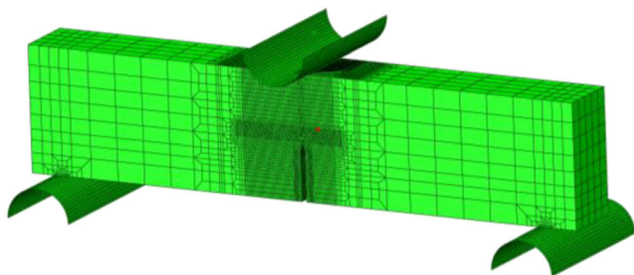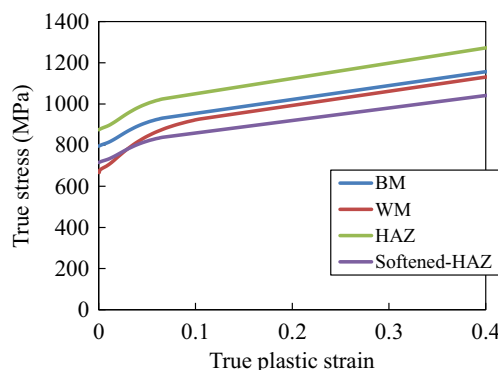

Fig. 13 True stress–true plastic strain curves of materials used for FEA

volume of the fracture process zone. The critical Weibull stress at a fracture initiation is known to be a material property independent of geometry and size of the specimen.

In this study, the shape parameter $m = 10$ was used, as specified in ISO 27306. The maximum principal stress of each element was used as σ_{eff}. The fracture process zone V_f was defined from the CGHAZ region where equivalent plastic strain takes place. A unit volume (1 mm^3) was chosen for V_0 because selection of the reference volume does not affect the value of m [14]. For the rest of the assessment in this study, $m = 10$ and $V_0 = 1$ were used.

3.2.3 Effect of crack front shape

The fatigue precrack had a snake-like shape in the thickness direction as shown in Fig. 10. The snake-like shape would affect the stress field on the crack tip because of stress concentration. Therefore, the effect of the crack front shape on the Weibull stress of the 3PB specimen was investigated prior to calculating the critical Weibull stress distribution.

Two 3PB models with different crack front shapes were used in the analyses as shown in Fig. 14. The crack front shape of one of the models was the actual initial shape (Y17), and the other model had a flat shape with a/W = 0.5.
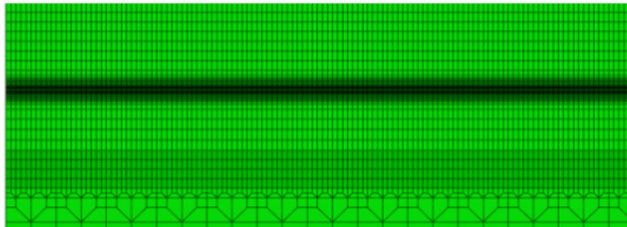
Figure 15 shows the analytical results. The Weibull stress for the model with the original crack front shape was larger than for the model with a/W = 0.5. Hence, the crack front shape must be set to the actual initial shape.

3.2.4 Calculating critical Weibull stress distribution

Prior to calculating the critical Weibull stress distribution, the validity of 3PB analysis was tested based on macroscopic deformation. Figure 16 shows a comparison of the load–CMOD curve between experimental and finite element method (FEM) results for Y16 (critical CTOD = 0.047 mm), Y17 (critical CTOD = 0.030 mm), and Y21 (critical CTOD = 0.054 mm). The analytical results were in good agreement with the experimental results, thus validating the analysis in terms of macroscopic deformation.

Fig. 12 FE model of 3PB specimen
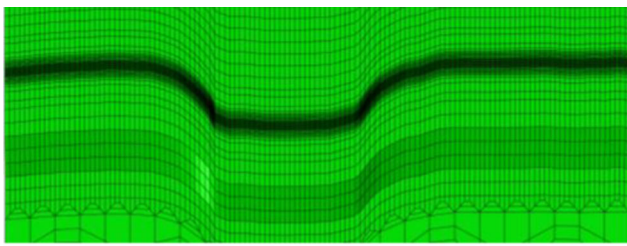
(a) Actual initial shape

(a) Flat shape, a/W = 0.5

Fig. 14 Crack front shape of FEM model. **a** Actual initial shape. **b** Flat shape, a/W = 0.5

Fig. 16 Comparison between EXP and FEM results for load–CMOD curve (Y16, 17, 21)

WP specimen with an embedded crack was estimated based on the critical Weibull stress distribution.

4.1 Analytical method

ABAQUS ver. 6.11.5 was used for FEA. Figure 18 shows the FE meshes used for the WP specimen. The embedded crack front shape was accurately modeled based on the fracture surface of the test specimen as shown in Fig. 19. The minimum element size at the crack tip was $0.025 \times 0.025 \times 0.2$ mm. Iso-parametric elements with eight nodes, C3D8, were employed. The analytical model was classified into four parts for material properties based on the hardening distribution shown in Fig. 6: the base metal, weld metal, HAZ, and softened HAZ.

Welding residual stress was introduced to the analytical model as shown in Fig. 20; the model was tensioned in the vertical direction to the weld line. The tension load, global displacement, and CTOD at the fracture initiation point were calculated. The tangential method was used to calculate CTOD.

Figure 17 shows the relationship between the Weibull stress and CTOD for each model. There were few differences for each analytical result because of the differences in the crack front shape and microstructure distribution. Table 5 lists the critical Weibull stress (maximum, minimum, and average values) calculated by the experimental critical CTOD and the relationship between the Weibull stress and CTOD for each model. From these results, the critical Weibull stress distribution of CGHAZ of the welded joint was obtained as 2110–2784 MPa.

4 Estimation of critical CTOD of WP tensile specimen with embedded crack

The critical Weibull stress distribution of CGHAZ was presented in the previous section. Here, the critical CTOD of the
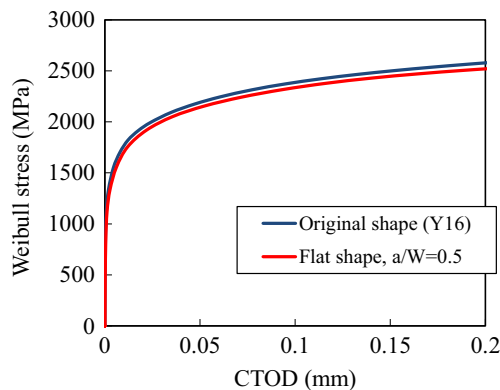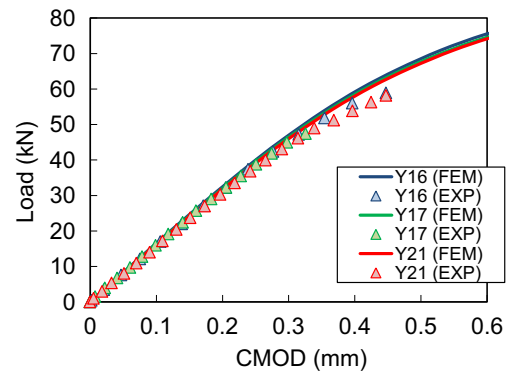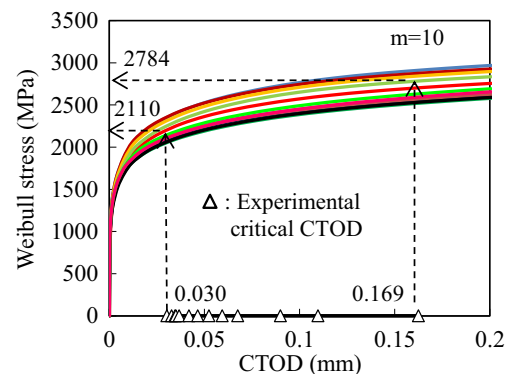

Fig. 15 Effects of crack front shape on Weibull stress for 3PB specimens

Fig. 17 Relationship between CTOD and Weibull stress for 3PB specimens fracturing in CGHAZ

Table 5   Calculated critical Weibull stress for CGHAZ

Critical Weibull stress (MPa)		Specimen
Maximum	2784	Y9 ($\delta_{cr} = 0.169$ mm)
Minimum	2110	Y17 ($\delta_{cr} = 0.030$ mm)
Average	2352	–
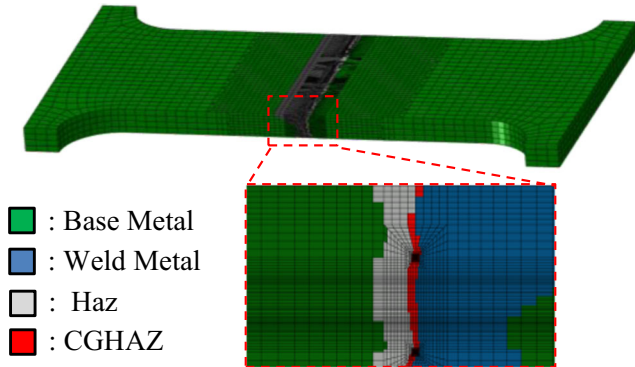
Fig. 18   FEM model for WP specimen

Fig. 20   Welding residual stress introduced to analytical model
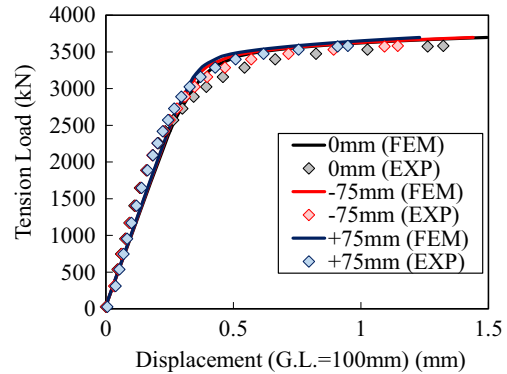
Fig. 21   Comparison between EXP and FEM results for load–displacement curve

4.2 Analytical results

Prior to calculating Weibull stress, the validity of the analysis was confirmed. Figure 21 shows a comparison of the load–global displacement curve between the experimental and FEM results. The good agreement between these two results confirmed the validity of the analysis in terms of macroscopic deformation.

Figure 22 shows the relationship between the Weibull stress and tension load, and Fig. 23 shows the relationship between the Weibull stress and global displacement. The predicted tension load and global displacement at brittle fracture were calculated from the critical Weibull stress distribution in Table 5. Table 6 gives a comparison between the experimental and predicted results. The brittle fracture limit for a welded joint with an embedded flaw generated by cold cracking could be predicted from the Weibull stress criterion because both the predicted fracture tension load and global displacement were in agreement with experimental results from the WP tension test.
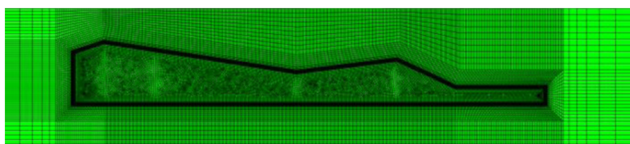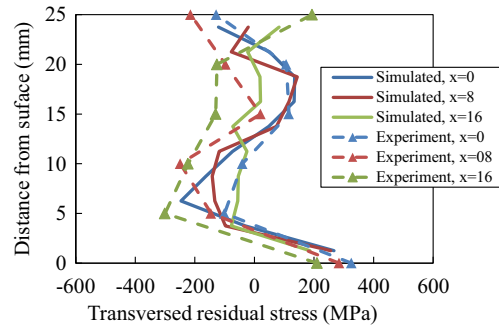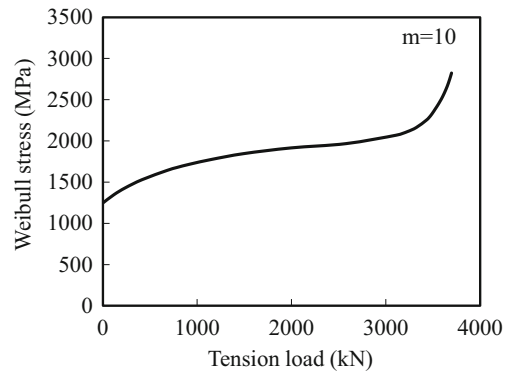

Fig. 22   Relationship between tension load and Weibull stress

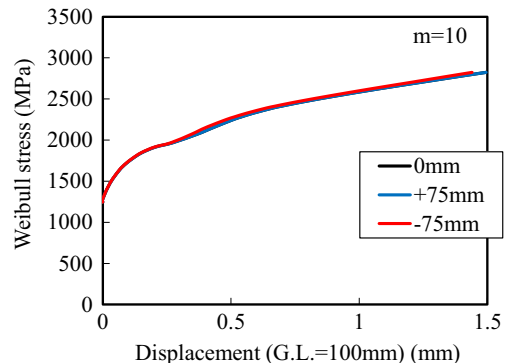Fig. 19   Embedded crack front shape for analytical model

Fig. 23   Relationship between global displacement and Weibull stress

Table 6 Comparison between experimental and predicted results for WP specimen

		Experimental result	Predicted result
Tension load (kN)		3584	3222–3687
Displacement (mm)	0	1.35	0.40–1.41
	75	1.17	0.37–1.36
	−75	0.97	0.36–1.17

Table 7 Analytical conditions

	Residual stress	Crack configuration
Case 1	Without	Original (see Fig. 19)
Case 2	With	

5 Effect of welding residual stress and crack configuration on Weibull stress for embedded flaw

5.1 Effect of welding residual stress

The effect of welding residual stress on the Weibull stress for WP specimens with an embedded flaw was evaluated because welding residual stress has a large effect on the brittle fracture limit of a welded joint. Two WP tension analyses with an embedded flaw were conducted using the conditions listed in Table 7. Distribution of the transverse residual stress introduced to the FEM model is shown in Fig. 24, similar to that shown in Fig. 20.

Figure 25 shows a comparison between a case without residual stress (case 1) and a case with residual stress (case 2). CTOD was calculated using the tangential method at the fracture initiation point shown in Fig. 4. The Weibull stress was increased by the welding residual stress up to CTOD = 0.15 mm. This result is in agreement with previously reported results for high-strength welded joint steels with
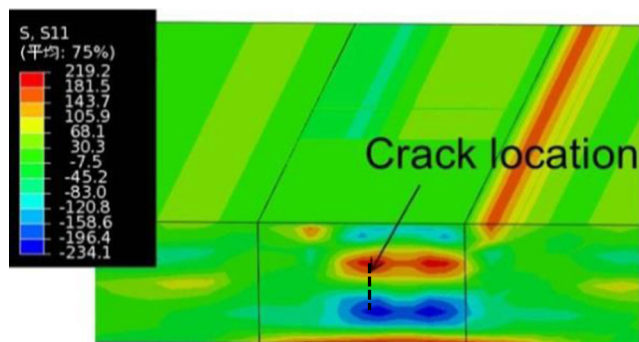

Fig. 24 Distribution of introduced transverse residual stress
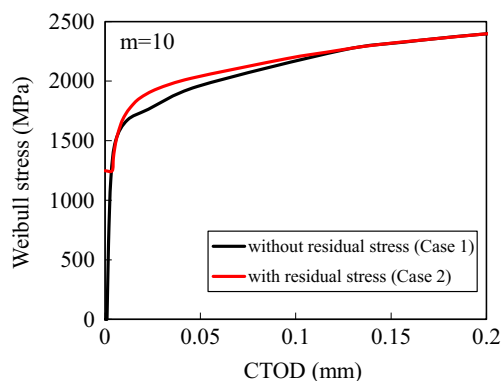

Fig. 25 Effect of residual stress on Weibull stress

residual stress [8]. Therefore, residual stress must be considered when conducting a WP tensile analysis.

5.2 Effect of crack configuration

An embedded flaw generated by cold cracking has a complex shape as shown in Fig. 4. The detected flaw is modeled as an idealized flaw for fracture assessment according to international standards such as BS7910. The crack configuration would affect the Weibull stress because the complex shape may increase the Weibull stress because of stress concentration. Therefore, two WP tension analyses with different crack configurations were conducted to clarify the effect of crack configuration. The crack configuration of each model is shown in Fig. 26. The maximum flaw height and flaw length of the idealized model were the same as those of the simulated model.
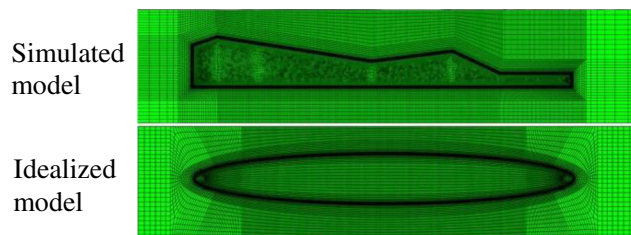

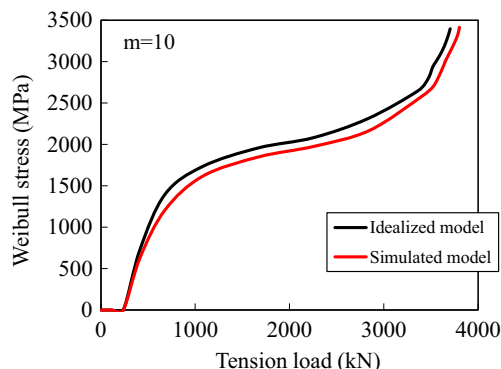**Fig. 26** Crack configuration for FEM models

Fig. 27 Effect of crack configuration on Weibull stress

Figure 27 shows the relationship between the Weibull stress and tension load. The Weibull stress of idealized model was larger than that of the simulated model in the entire tension load region. It was confirmed that there was no effect of stress concentration on the Weibull stress in the case of this embedded crack configuration.

6 Conclusion

The brittle fracture limit of a welded joint with an embedded flaw was investigated by conducting experiments and FEAs using the Weibull stress criterion. The following results were obtained:

1. A WP tensile test with an embedded flaw was conducted at −30 °C. Brittle fracture occurred in CGHAZ when the tension load was 3584 kN.
2. The brittle fracture limit of a welded joint with an embedded flaw generated by cold cracking can be estimated from the results of 3PB tests with fatigue crack based on the Weibull stress criterion.
3. The Weibull stress of welded joint with an embedded flaw was increased by the welding residual stress. There was no effect of stress concentration on the Weibull stress in the case of this embedded crack configuration.

References

1. BS7910:2013 (2013) Guide to methods for assessing the acceptability of flaws in metallic structures, British Standard Institution
2. WES2805-2011 (2011) Method of assessment for flaws in fusion welded joints with respect to brittle fracture and fatigue crack growth, The Japan Welding Engineering Society
3. Beremin FM (1983) A local criterion for cleavage fracture of a nuclear pressure vessel steel. Metall Trans A 14A:2277–2287
4. Mudry F (1987) A local approach to cleavage fracture. Nucl Eng Des 105:65–76
5. ISO27306 (2009) Method of constraint loss correction of CTOD fracture toughness for fracture assessment of steel components
6. Minami F (1996) Fracture toughness requirement for fracture performance evaluation of welded joints based on the local approach, Proceedings of the International Conference on Offshore Mechanics and Arctic Engineering. pp 193–202
7. Minami F (1997) Prediction of specimen geometry effect on fracture resistance of HAZ-notched welds by local approach. Mis-Matching Interfaces Welds 319–330
8. Yamashita Y (2010) Constraint loss correction for assessment of CTOD fracture toughness under welding residual stress. Part 1 Methodol Eng Fract Mech
9. Imai Y (2014) Fracture evaluation of welded joints with embedded flaw from cold cracking. Weld Struct Symp. (in Japanese)
10. Lu J, James M, Roy G (eds) (1996) Handbook of measurement of residual stress. The Fairmont Press, Inc., Lilburn, Georgia, USA
11. BS7448 (1991) Fracture mechanics toughness tests, part 1, British Standard Institution
12. API Recommended Practice 2Z (2005) Recommended practice for preproduction qualification for steel plates for offshore structures
13. Seko Y (2015) Application of Weibull stress criterion to brittle fracture assessment of HAZ-notched welds with residual stress. J Press Vessel Technol 138(2)
14. Minami F (1992) Estimation procedure for the Weibull parameter used in the local approach. Int J Fract 54:197–210